Electrostatic Interactions in an Integral Membrane Protein†

E. T. Johnson and W. W. Parson*

Department of Biochemistry, Box 357350, University of Washington, Seattle, Washington 98195-7350

Received December 7, 2001; Revised Manuscript Received March 20, 2002

ABSTRACT: The effects of charge−charge interactions on the midpoint reduction potential (E_m) of the primary electron donor (P) in the photosynthetic reaction center of *Rhodobacter sphaeroides* were investigated by introducing mutations of ionizable amino acids at selected sites. The mutations were designed to alter the electrostatic environment of P, a bacteriochlorophyll dimer, without greatly affecting its structure or molecular orbitals. Two arginine residues at homologous positions in the L and M subunits [residues (L135) and (M164)], Asp (L155), Tyr (L164), and Cys (L247) were changed independently. Arginine (L135) was replaced by Lys, Leu, Gln, or Glu; Arg (M164), by Leu or Glu; Asp (L155), by Asn; Tyr (L164), by Phe; and Cys (L247), by Lys or Asp. The R(L135)E/C(L247)K double mutant also was made. The shift in the E_m of P/P^+ was measured in each mutant and was compared with the effect predicted by electrostatics calculations using several different computational approaches. A simple distance-dependent dielectric screening factor reproduced the effects remarkably well. By contrast, microscopic methods that considered the reaction field in the protein and solvent but did not include explicit counterions overestimated the changes in the E_m considerably. Including counterions for the charged residues reduced the calculated effects of the mutations in molecular dynamics calculations. The results show that electrostatic interactions of P with ionizable amino acid residues are strongly screened, and suggest that counterions make major contributions to this screening. The screening also could reflect penetration of water or other relaxations not taken into account because of incomplete sampling of configurational space.

The dielectric screening that determines the strength of interaction between two charged or polar species in a protein is a complicated function of the protein structure and the solvent. Because most globular proteins fold with hydrophobic amino acid residues inside and ionizable residues on the surface, it frequently is suggested that the protein interior has a low dielectric constant on the order of 4 (*1*). However, experimental work even 20 years ago indicated that the dielectric screening of charged groups in proteins often is much stronger than this. Early measurements of the shifts of the midpoint reduction potential (E_m)[1] in a series of cytochrome *c* derivatives with chemically modified lysine residues showed that the effective dielectric screening factor for surface groups was approximately 50 (*2*). In a more recent study, Zhou and Swenson examined the interactions of a partially buried flavin group with six Glu and Asp residues in a flavodoxin (*3*). All the ionizable groups were on the protein surface, and were within 13 Å of N1 of the flavin. Replacing one of the Glu or Asp residues by a nonionizable amino acid raised the E_m of the $FMNH^-/FMNH^\bullet$ couple by an average of only about 15 mV per unit change in charge. In this case, the effective dielectric screening factor was in the range of 50−100, depending on the location of the charged residue.

Lockhart and Kim (*4*) have examined the effects of permanent charges and dipoles on the pK_as of ionizable residues in helical model peptides. They found that long-range interactions with permanent charges were strongly screened, and they concluded that the pK_as of ionizable residues were determined mainly by dipolar interactions with the helical backbone. Similarly, Forsyth and Robertson (*5*) have described the effects of a particular Lys residue on the pK_as of several Asp and Glu residues in turkey ovomucoid third domain. Previous calculations (*6*) had suggested that the pK_as of these residues were sensitive to interactions with the Lys; however, replacing the Lys by Thr or Glu had little or no measurable effect on the pK_a of any of the acidic acids.

Complementary studies have shown that buried ionizable amino acids can be charged. The arabinose binding protein, for example, has a charged Arg that is not accessible to solvent but is stabilized through hydrogen bonds (*7*). Lysozyme has an ionized Asp that is stabilized similarly (*8, 9*). Hydrogen bonds also appear to stabilize the buried chromophore of the photoactive yellow protein in a charged state (*10*). Localized dipoles near the ends of α-helices stabilize charged groups in barnase and a sulfate binding protein (*11*). Mutation of a Val to Asp or Glu adjacent to the heme in myoglobin leads to an ionized amino acid that is stabilized by the positive charge on the heme iron and shifts the E_m of the heme by about −200 mV (*12, 13*). Garcia-Moreno et al. have inserted either a Lys or a Glu into the hydrophobic core of a nuclease and determined the pK_a of the buried group from difference potentiometry and measurements of protein stability (*14, 15*). The ionized

† This work was supported by National Science Foundation Grant MCB-9904618 and by a Molecular Biophysics Training Grant (GM08268) from the National Institutes of Health.

* Corresponding author. E-mail: parsonb@u.washington.edu.

[1] Abbreviations: E_m, reduction potential; RC, photosynthetic reaction center; PDLD, Protein-Dipole Langevin-Dipole; SEM, standard error of the mean.

10.1021/bi012131y CCC: $22.00
Published on Web 04/26/2002

residues did not unfold the protein and appeared to be stabilized by interactions with protein dipoles and water molecules. Williams et al. (*16*) recently showed that ionized Asp and Glu residues could be introduced at several buried sites in photosynthetic bacterial reaction centers without disrupting the protein.

Attempts to calculate the energies of electrostatic interactions in proteins have met with mixed success. There are two main applications for such electrostatics calculations. The first is to calculate the self-energy of a system, defined as the solvation free energy of a group of atoms (e.g., a bound cofactor or the reacting functional groups at one step of an enzymatic reaction) in the absence of interactions with other charged groups. The second application is to evaluate the electrostatic interactions between separate charged groups. Warshel and co-workers have noted that semimacroscopic calculations require a larger effective dielectric constant for interactions of charged groups than for self-energies (*17*−*19*). They argue that the use of a macroscopic dielectric constant (ϵ) with any value other than 1 simply compensates for factors that are not treated explicitly. A treatment that does not consider structural relaxations, for example, usually requires a larger dielectric constant than one that allows the structure to fluctuate. However, calculations of the self-energies of charged groups in proteins appear to have become reasonably accurate, even though the dielectric constant used for the protein interior (ϵ_{in}) may have no simple physical interpretation (*19*−*25*). Using free energy perturbation techniques, Cutler et al. (*26*) were able to account well for the effect of an Arg to Leu mutation on the pK_a of a heme propionate group in cytochrome *c*. Fersht et al. (*27*−*29*) have studied surface charge−charge interactions in barnase and subtilisin by constructing a series of basic mutations and measuring the change in the pK_a of a histidine residue. The histidine and the sites of the mutations were on the protein surface, and the measured interaction energies were small (0.3−0.5 kcal/mol for groups separated by 12−17 Å). In this case, the experimental results were reproduced well by continuum electrostatics calculations with a value of 2 for ϵ_{in} and a dielectric constant of 80 for the solvent (ϵ_{out}) (*29*). Antosiewicz et al. (*30*), however, found that calculations of the pK_as of ionizable residues in a large group of proteins required a substantially higher value of ϵ_{in}. The best fit to the data was obtained by using $\epsilon_{in} \approx 20$ for both self-energies and charge−charge interactions, suggesting that significant components are missing from the analysis.

Recently, there has been much effort to consider protein relaxations in electrostatics calculations. Sham et al. (*17*) have evaluated the effects of relaxations by calculating the interaction energies of pairs of ionizable residues during molecular dynamics trajectories in the charged and uncharged states and comparing the results to those of calculations with the unrelaxed crystallographic structure. Alexov et al. (*20, 24, 25, 31*) have used a Monte Carlo procedure that considers many configurations of the polar hydrogens. These workers also considered the variation of heavy-atom positions in families of crystal structures for the same protein. Nielsen et al. (*32*) have emphasized the effects of hydrogen-bonding networks and of flipping amino acid side chains.

Most of the studies cited above have involved water-soluble proteins. Much less is known about the screening of electrostatic interactions in the interior of integral membrane proteins. The photosynthetic reaction center (RC) of *Rhodobacter sphaeroides* provides an excellent model for studying electrostatic interactions in such a protein. The RC contains two homologous polypeptides (L and M), each of which has five transmembrane α-helices, a third polypeptide (H) with one transmembrane helix, four bacteriochlorophylls (P_L, P_M, B_L, and B_M), two bacteriopheophytins (H_L and H_M), and two quinones (Q_A and Q_B) [see (*33*) for a review]. Two of the bacteriochlorophylls (P_L and P_M) form a strongly interacting dimer (P) that releases an electron when the RC is excited with light. The electron moves to one of the quinones (Q_A) by way of B_L and H_L. The rapid kinetics and high specificity of the electron-transfer reactions depend in part on the relative energies of the excited state (P*) and charge-separated states such as $P^+B_L^-$ and $P^+B_M^-$. It has been suggested that long-range electrostatic interactions with charged residues poise the energies of these states such that electron transfer to B_L and H_L is more favorable than transfer to B_M and H_M (*34*). Other studies, however, have suggested that the interactions of the electron carriers with ionizable residues are strongly screened and make only minor contributions to the energies (*35*).

Electrostatic interactions with the protein would be expected to play a role in determining the E_m of the P/P^+ couple and the energies of charge-transfer states such as $P_L^+P_M^-$, which influence the spectroscopic properties of the RC. Williams, Allen, and co-workers have described an extensive series of mutations that introduce or remove hydrogen bonds to the acetyl and keto groups of P_L and P_M (*36*−*39*). Each hydrogen bond raises the E_m of P by 50−100 mV. The effects are additive, and double and triple mutants are able to alter the redox properties of the dimer significantly. Muegge et al. (*22*) were able to reproduce the effects of many of these mutations on the E_m by continuum electrostatics calculations. However, the effects of such mutations cannot necessarily be attributed purely to electrostatic interactions. Changes in hydrogen bonding could alter the molecular orbitals of P_L and P_M or cause small shifts in the positions of the molecules, either of which could affect the E_m through changes in the resonance interactions of the two bacteriochlorophylls.

In the current work, we have mutated a series of ionizable residues that are close enough to P to affect its electrostatic potential, but sufficiently far away so that the mutations are unlikely to cause major changes in the positions or molecular orbitals of the bacteriochlorophylls. Most of the mutation sites are largely buried in the protein. Changing the charges at these sites stabilizes or destabilizes P^+ relative to P, as measured by shifts in the E_m of P/P^+. The changes in the E_m are compared to the effects predicted by several different computational approaches, and the merits of these methods are discussed.

MATERIALS AND METHODS

Construction and Purification of Mutant RCs. Oligonucleotide-mediated site-directed mutagenesis was accomplished with the Chameleon Kit (Stratagene) for the initial mutations of Leu and Glu at both R(L135) and R(M164) and the Quikchange Kit (Stratagene) for the balance of the mutations. The mutagenesis was performed in puc18 or puc19 vectors containing portions of the L or M subunits, following

methods developed by Williams et al. (*36*, *40*, *41*). After transformation into *Escherichia coli* strain DH5α cells and purification of the mutated plasmid DNA, the regions containing the mutations were subcloned into the *puc* operon. The R(M164) mutations were cloned into the pRKSCH vector (*41*). The R(L135), D(L155), Y(L164), and C(L247) mutations were cloned into the pRKSCH/pHis vector, which contains a tail of seven histidine residues at the carboxyl terminal of the M-subunit (*42*). The plasmids were transformed into the *E. coli* strain S-17 and conjugated with ΔLM1.1, a *Rb. sphaeroides* strain that has the RC deleted (*40*). DNA from the mutant RC-complemented ΔLM1.1 strains was purified and sequenced to ensure that the mutations had been introduced correctly.

Wild-type and mutant *Rb. sphaeroides* strains were grown semi-aerobically in rich media for 3−5 days in the dark (*40*). RCs from the R(M164) mutants were isolated by standard procedures (*43*, *44*) with minor modifications. The solubilization of the RCs was achieved with 0.65% *N*,*N*-dimethyldodecylamine-*N*-oxide (LDAO, Fluka), a slightly lower concentration than the 1.2% used by Feher and Okamura (*43*), and after ultracentrifugation, the supernatant was brought to 1% LDAO and 30% NH_4SO_4 (w/v) to precipitate the RCs. The Celite step was omitted, and the solubilized floating pellet was dialyzed to remove salts and loaded onto a DEAE column. The RCs were eluted with a gradient of 0.03−0.25 M NaCl. RCs from the R(L135), D(L155), Y(L164), and C(L247) mutations were isolated using a protocol that exploited the histidine tag (*42*), and were purified further by chromatography on DEAE-Sepharose (Bio-Rad). The purified RCs were dialyzed against 15 mM Tris-HCl, pH 8, 0.025% LDAO, and 1 mM EDTA and concentrated to an OD_{800} of 40 in a 1 cm cuvette using an Amicon pressure cell or a Centricon-50 filter device. The purity of the sample was measured by the ratio OD_{280}/OD_{800} and typically was between 1.4 and 1.8.

Redox Potential Measurements. The P/P^+ midpoint redox potential (E_m) was measured with an electrochemical cell essentially as described by Nagarajan et al. (*45*). The gold-mesh working electrode had 333 lines/in. and was modified with 4,4′-dithiodipyridine. The RCs were suspended in 20 mM Tris, pH 8, 0.1% LDAO, 1 mM EDTA, 60 mM KCl, with 0.25 mM K^+ ferrocyanide and 0.15 mM K^+ tetracyanomono(1,10-phenanthroline)ferrate(II) tetrahydrate as redox mediators. The absorbance of P at the peak of the long-wavelength absorption band (865 nm for wild-type RCs, but shorter wavelengths for some of the mutants) was monitored as a function of the applied potential. A nonlinear least-squares procedure was used to fit the data to the one-electron Nernst equation:

$$[P]/[P^+] = (A - A_{ox})/(A_{red} - A) = \exp\{0.03894(E_m - E)\} \quad (1)$$

where A, A_{ox}, and A_{red} are, respectively, the absorbance measured at potential E and at potentials well above and well below the E_m. The E_m of wild-type RCs was measured along with each measurement on a mutant strain, and the shift of the E_m in the mutant was referenced to the wild-type E_m. Oxidative and reductive titrations were fit separately and averaged, and the shifts quoted below for a given mutant are the mean of between 3 and 5 measurements. Potentials are given in millivolts relative to the hydrogen electrode at pH 7.0.

Models for Electrostatics Calculations. Assuming that the mutation does not affect the gas-phase (molecular orbital) energy difference between P^+ and P, the change in E_m caused by a mutation (ΔE_m) should be proportional to the change in ΔG_{sol}, the difference between the free energies of solvation of P^+ and P by the surrounding protein, water, and electrolytes ($\Delta G_{sol} = G_{sol}^{P^+} - G_{sol}^{P}$):

$$\Delta E_m = -\frac{1}{nF}\Delta\{G_{sol}^{P^+} - G_{sol}^{P}\} \equiv -\frac{1}{nF}\Delta\Delta G_{sol} \quad (2)$$

where F is the Faraday constant (23.06 kcal mol^{-1} V^{-1}) and $n = 1$. We calculated $\Delta\Delta G_{sol}$ by several different approaches, using structural models based on the crystal structure of *Rb. sphaeroides* RCs described by Ermler et al. (*46*) [Protein DataBank (*47*) file 1pcr]. Mutations were introduced by replacing the side chain of the wild-type residue starting with C_γ, using a Monte Carlo procedure to minimize the torsional, electrostatic, and van der Waals energies of the new side chain (*48*). The polar hydrogens of the 108 Ser, Thr, and Tyr residues and the 158 crystallographic water molecules (a total of 424 rotatable hydrogens) were oriented initially to optimize the networks of hydrogen bonds, and then were rotated to minimize the total electrostatic, van der Waals, and torsional energy of the model. The latter minimization was done by a Metropolis Monte Carlo, simulated-annealing procedure, in which the temperature was decreased from 1000 to 10 K in 20 steps; 8480 (20 × 424) random moves were made at each step.

The simulated-annealing procedure was carried out 5 times for each oxidation state of P (P and P^+) in order to generate separate sets of low-energy protein configurations for each oxidation state. We then evaluated ΔG_{sol} with the linear-response approximation (*49*−*52*):

$$\Delta G_{sol} = \frac{1}{2}\{\langle\Delta V_{sol}\rangle_P + \langle\Delta V_{sol}\rangle_{P^+}\} \quad (3)$$

where ΔV_{sol} is the difference between the calculated solvation energies of P^+ and P for a given configuration of the protein ($\Delta V_{sol} = V_{sol}^{P^+} - V_{sol}^{P}$) and $\langle\cdots\rangle_i$ denotes the mean of the values for configurations of electronic state i. The LRA incorporates a major component of the dipolar reorganization of the protein in response to a change in the charge on P. ΔV_{sol} was calculated by a variety of approaches as described below. In the molecular dynamics calculations, $\langle\cdots\rangle_i$ becomes an average over a trajectory in state i.

The atomic charges for the protein were taken from the ENZYMIX force field (*53*); those of the bacteriochlorophylls and bacteriopheophytins were obtained by the program QCFF/PI (*54*) and were the same as those used in previous calculations of spectroscopic properties of P^+ (*55*). Because the charges are spread over large π-electron systems and all the mutation sites are at least 8 Å from the centers of P_L and P_M, the calculated solvation energies do not depend stongly on the details of the intramolecular charge distribution (*56*). The calculated effects of the mutations did, however, depend to some extent on the division of the net positive charge of P^+ between P_L and P_M. Except where

stated otherwise, the net charge was divided equally between the two bacteriochlorophylls.

Equation 2 involves a significant approximation because a complete treatment of the E_m requires considering quantum mechanical electronic and vibronic coupling of P_L and P_M. This can be done by describing P^+ as a linear combination of the basis states $P_L{}^+P_M$ and $P_LP_M{}^+$, whose energies are sensitive to mutations of residues near the pigments (*38, 39, 57*). The E_m is obtained by diagonalizing the interaction Hamiltonian, in which the electronic and vibronic coupling factors enter mainly as off-diagonal matrix elements. Calculations of this type, carried out using the formalism described by Gasyna and Schatz (*58*), showed that the changes in the E_m are related predominantly to changes of the basis state energies and are relatively insensitive to the electronic and vibronic coupling factors. The simple treatment expressed by eq 2 thus appears to be an acceptable approximation for our present purposes. The quantum calculations will be presented elsewhere, along with measurements on the ENDOR and FTIR spectra of the mutant RCs (E. T. Johnson, W. W. Parson, F. Müh, W. Lubitz, J. C. Williams, J. P. Allen, J. Breton, and E. Nabedryk, unpublished experiments).

PDLD Calculations. The Protein-Dipole Langevin-Dipole (PDLD) method treats dielectric screening by including a self-consistent set of induced dipoles on the non-hydrogen protein atoms and a grid of points representing the surrounding medium (*21, 35, 59*). The total solvation energy for $P \rightarrow P^+$ in structural models relaxed in oxidation state i is written

$$\Delta V_{sol} = \Delta V_{Q\mu} + \Delta V_{ind} + \Delta V_{H_2O} + \Delta V_{memb} + \Delta V_{bulk} \quad (4)$$

Here $\Delta V_{Q\mu}$ ($\Delta V_{Q\mu} \equiv V_{Q\mu}^{P^+} - V_{Q\mu}^{P}$) is the difference between the energies of electrostatic interactions of P and P^+ with the other partial charges of the protein and pigment atoms, calculated with $\epsilon = 1$, and ΔV_{ind}, ΔV_{H_2O}, ΔV_{memb}, and ΔV_{bulk} are, respectively, the corresponding differences in the energy of interactions with induced dipoles in the protein, water, membrane, and the bulk solvent outside the region that is treated microscopically. The protein model for these calculations was trimmed to a 32 Å sphere centered on P, and retained most of the RC (approximately 10 000 atoms).

The induced dipole at any atom or grid point depends on the electric field at that point and on the polarizability of the volume element represented by the point. Because the field at any point includes both the static field of the protein atoms and the field from the other induced dipoles, an iterative procedure is used to obtain a self-consistent solution. We set the polarizability of the protein atoms to correspond to the macroscopic polarizability of a homogeneous medium with a dielectric constant of ~2.2 according to the Clausius-Mosotti equation (*56*). The grid points representing the surrounding medium had a spacing of 2 Å and were divided into water and membrane regions as described by Alden et al. (*35*). In most of the calculations, the membrane region was 25 Å thick and had a polarizability corresponding to a macroscopic dielectric constant of 4, while the water region had a higher polarizability that modeled the low-frequency dielectric behavior of liquid water (*35*).

PDLD/S Calculations. In the PDLD/S method, the protein's induced dipoles are treated implicitly by introducing an effective dielectric screening factor (ϵ_{in}) for the interactions with fixed charges of the protein atoms, while the solvent dipoles are evaluated explicitly on a cubic grid as in PDLD (*17, 53*). The solvation energy in this model is

$$\Delta V_{sol} = \frac{\Delta V_{Q\mu}}{\epsilon_{in}} + (\Delta V_{H_2O} + \Delta V_{memb} + \Delta V_{bulk})\left(\frac{1}{\epsilon_{in}} - \frac{1}{\epsilon_{out}}\right) \quad (5)$$

where ϵ_{out} is the dielectric constant of the solvent and the other quantities are as in eq 4. For these calculations, we set $\epsilon_{out} = 80$ and varied ϵ_{in} between 2 and 20.

Poisson−Boltzmann (DelPhi) Calculations. In the Poisson−Boltzmann or discretized-continuum method, as implemented in the program DelPhi (*60−62*), the protein−solvent system is mapped to a cubic grid with two dielectric regions. The region corresponding to the protein has an adjustable dielectric constant of ϵ_{in}, and that corresponding to the solvent usually is given a dielectric constant (ϵ_{out}) of 80. The reaction field induced by the charges of the protein and pigment atoms is evaluated by the linearized Poisson−Boltzmann equation with the boundary condition that the potential goes to that described by Debye−Huckel theory at large distances from the protein. Coulombic interactions ($\Delta V_{Q\mu}$ in our notation) are evaluated after the atomic charges are distributed onto the grid, and are screened by ϵ_{in} as in PDLD/S. The total solvation energy takes the form

$$\Delta V_{sol} = \frac{\Delta V_{Q\mu}}{\epsilon_{in}} + \Delta V_{RF} \quad (6)$$

where ΔV_{RF} is the difference between the reaction-field energies in the states P and P^+. To include a membrane in the discretized-continuum calculations, pseudo-protein atoms with no charges were added to fill a 25 Å region similar to the membrane region described above. This effectively removes solvent from the membrane region and gives this region the same ϵ_{in} as the protein. The boundary conditions for the potential were treated by using three grids that successively focused down on the protein to a final resolution of 2.4 grid points/Å. The protein filled 20% of the first grid, 85% of the second, and 90% of the third. The PARSE dataset (*63*) was used for the atomic radii.

Calculations Using Distance-Dependent Screening Factors. In these calculations, charge−charge interactions between atoms i and j are screened by an empirical function of the interatomic distance [$f_{ij}(r_{ij})$]. The difference in solvation energies between P^+ and P becomes simply

$$\Delta V_{sol} = \sum_{i}^{\text{atoms of P}} (Q_i^{P^+} - Q_i^{P}) \sum_{j}^{\text{other atoms}} \frac{q_j}{f_{ij} r_{ij}} \quad (7)$$

where Q_i and q_j are the partial charges on atom i of P_L or P_M and atom j of the protein or a crystallographic water and r_{ij} is the distance between atoms i and j. The entire protein was included in these calculations.

Several different expressions for f_{ij} were considered. The expression introduced by Warshel et al. (*64*) for modeling shifts of E_m and pK_a values has an exponential dependence on distance:

$$f_{ij} = 1 + 60(1 - e^{-\eta r_{ij}}) \quad (8)$$

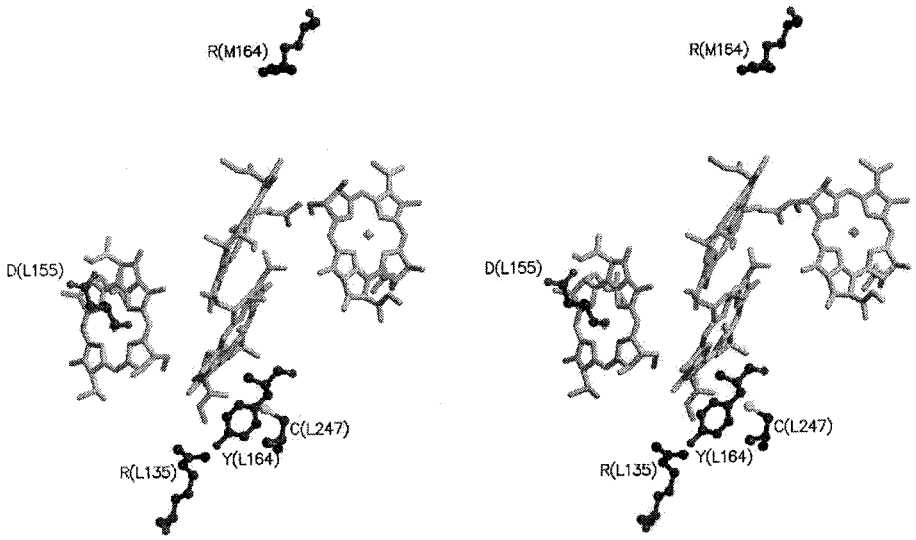

FIGURE 1: Stereoview of the bacteriochlorophylls and the mutation sites in the photosynthetic reaction center of *Rb. sphaeroides* (*46*). The phytol side chains of the bacteriochlorophylls are removed for clarity. The view is approximately along the C_2 pseudosymmetry axis. The figure was prepared with Molscript (*85*) and Raster3D (*86*).

where η is an empirical factor in the range of 0.10−0.18. We also tried a simple linear dependence on distance, $f_{ij} = r_{ij}$, and a sigmoidal dependence of the form (*65*−*67*):

$$f_{ij} = \epsilon_{out} - \frac{\epsilon_{out}}{2}[(r_{ij}s)^2 + 2r_{ij}s + 2]e^{-r_{ij}s} \qquad (9)$$

with $\epsilon_{out} = 78$ and s (a sigmoidicity parameter) $= 0.3$.

Molecular Dynamics (MD) Simulations. To examine possible effects of protein backbone reorganization on the E_m of P/P^+, we carried out MD simulations using a slightly modified version of the program ENZYMIX (*53*, *68*). The crystal structure was trimmed to a 25 Å radius around the point midway between P and the ionizable group of the mutated residue, and unconstrained motions were allowed within 18 Å of this point. Atoms in the shell between 18 and 25 Å were constrained to their crystallographic coordinates, but were included in the electrostatics calculations. ΔV_{sol} was calculated during the MD trajectories essentially by eq 4, except that no membrane was included in this model and the Langevin dipoles were replaced by explicit water molecules. Waters were added as needed to fill the region with a radius of 20 Å and were modeled by the surface-constrained-all-atom-solvent (SCAAS) treatment (*69*). The Local Reaction Field method (*70*) with no distance cutoff was used to evaluate all charge−charge interactions.

Separate MD trajectories were propagated on the potential surfaces of P and P^+, with the charge of P^+ distributed equally between P_L and P_M. The structural model for each mutant was equilibrated during a 25 ps preliminary trajectory with P in a given state, and ΔV_{sol} then was recorded every 10 fs during a 100 ps trajectory with time steps of 1 fs. ΔG_{sol} was calculated from $\langle \Delta V_{sol} \rangle_P$ and $\langle \Delta V_{sol} \rangle_{P^+}$ by the LRA expression (eq 3). The MD calculations also provide the reorganization energy by the expression (*49*, *52*):

$$\lambda = \frac{1}{2}\{|\langle \Delta V_{sol} \rangle_P - \langle \Delta V_{sol} \rangle_{P^+}|\} \qquad (10)$$

Effects of counterions in the MD simulations were examined by including a single Na^+ or Cl^- ion in the water near the charged amino acid, so as to make the net charge of the system zero when P was in its reduced state. No additional counterion was added for P^+. One would expect a counterion for P^+ to have similar effects in the wild-type and mutant RCs, and so to make only small contributions to ΔE_m. However, because P is relatively far from the solvent-accessible surface of the protein, it provides little constraint on the location of a counterion in the solvent, and very long MD trajectories would be required in order for the solvation energy of the counterion to converge. For trajectories of the length used here (100 ps), the fluctuations of this solvation energy are large relative to the energy differences of interest. Molecular dynamics simulations of the L(247) mutations were not stable, again suggesting that the trajectories were too short to reorganize the counterion and surrounding protein around a completely buried charge.

RESULTS

Mutation Sites. Figure 1 shows the locations of the five residues we mutated to explore long-range electrostatic interactions of the protein with P. Arginines L135 and M164 are homologous residues of the L and M subunits, and are almost symmetrically positioned on either side of P. The C_ζ atom of R(L135) is 12.2 Å from the Mg of P_L and 19.5 Å from the Mg of P_M, while the C_ζ of R(M164) is 13.8 Å from the Mg of P_M and 21.0 Å from that of P_L. Although the arginines are located near the periplasmic surface of the RC, their side chains are almost completely buried. The sum of the solvent-accessible surface areas (*71*) for the guanidinium NH1 and NH2 nitrogens of R(L135) is 5.3 $Å^2$, and that for R(M164) is only 0.1 $Å^2$. In a fully exposed side chain, these atoms would have a total solvent-accessible surface of approximately 75 $Å^2$. R(L135) and R(M164) are located one turn from the carboxyl end of a transmembrane α-helix, which could stabilize a positive charge on the side chains. The charge on R(L135) also could be stabilized by hydrogen bonds to Y(L164) and a crystallographic water, while R(M164) could form a salt bridge with E(M173). Several peptide carbonyl groups also are oriented to stabilize positive charges at these locations. In addition, there are small pockets on the protein surface that could allow a counterion to sit

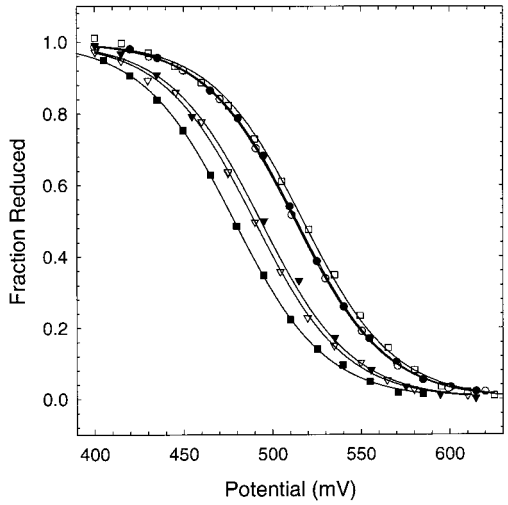

FIGURE 2: Representative redox titrations of P/P^+ in purified Y(L164)F (□), wild-type (●), R(L135)K (○), R(L135)L (▼), R(L135)Q (▽), and R(L135)E (■) RCs. The lines are best fits to the one-electron Nernst equation. The mean value of ΔE_m for each mutation is given in Table 1.

close to the guanidinium group of each arginine. The guanidinium groups also are close to, but not within hydrogen-bonding distance of, the keto oxygen atom of either P_L or P_M: these distances are 7.3 Å for R(L135) and P_L and 9.2 Å for R(M164) and P_M.

The carboxyl group of Asp (L155) is located approximately 14 Å from the Mg atoms of P_L and P_M. This residue is well exposed to the solvent, giving the γ-carboxyl group 45 Å^2 of accessible surface. The sulfur of Cys (L247) is 6.5 Å from the Mg of P_L and is completely inaccessible to the solvent.

E_m Values. Figure 2 shows representative redox titrations of P in the mutants of R(L135), and Table 1 gives the measured shifts of the E_m (ΔE_m^{expt}) for all the mutants relative to wild-type RCs. The conservative mutations R(L135)K and Y(L164)F have only marginal effects, shifting the E_m by −3 and +2 mV, respectively. The balance of the mutations of Arg (L135) replace a side chain that likely is positively charged by a neutral or negatively charged side chain. These substitutions all lower the E_m: Leu shifts the E_m by −20 mV; Gln, by −23 mV; and Glu, by −36 mV. The similar effects of leucine and glutamine, which are both neutral but differ in polarity, suggest that the shift results mainly from the loss of the positive charge of the Arg. The slightly larger effect of Gln, though not statistically significant, could possibly reflect a weak stabilization of P^+ by the dipole of the δ-amide group. Glutamic acid shifts the E_m by nearly twice as much as Leu, as would be expected if its δ-carboxylic acid group is negatively charged.

Mutations of Arg (M164) to neutral or negatively charged residues also decrease the E_m; however, the shifts are consistently about 4 mV smaller than those caused by homologous mutations of (L135). The Leu and Glu mutations shift the E_m by −16 and −32 mV. This is consistent with the slightly longer distance between Arg (M164) and P (see above), and with earlier evidence that the positive charge of P^+ is distributed unequally between P_L and P_M, with the larger share going to P_L (*44*) (see below).

The D(L155)N mutation raises the E_m by 12 mV, consistent with a destabilization of P^+ by removal of a negative charge. Cysteine (L247) also was mutated to Lys and Asp to explore the effects of replacing a neutral residue by a positively or negatively charged amino acid; the C(L247)K mutation increases the E_m by 51 mV, and the C(L247)D mutation decreases it by 40 mV. The double mutation R(L135)E/C(L247)K changes the E_m by +8 mV, which is a nearly additive combination of the individual effects.

Table 1: Measured Shifts in the E_m of P/P^+ in Mutant RCs and Shifts Calculated by PDLD and DelPhi with the Linear Response Approximation[a]

strain	ΔE_m^{expt}	ΔE_m^{calc} (PDLD)[b]	ΔE_m^{calc} (DelPhi)[c]
R(L135)K	−3	−6	+10
R(L135)L	−20	−98	−101
R(L135)Q	−24	−128	−121
R(L135)E	−37	−194	−238
D(L155)N	+12	+100	+81
Y(L164)F	+2	−58	−41
R(M164)L	−16	−56	−114
R(M164)E	−32	−147	−261
C(L247)K	+51	+332	+341
C(L247)D	−40	−346	−315
R(L135)E/C(L247)K	+8	+291	+211

[a] ΔE_m^{expt} and ΔE_m^{calc} are the measured and calculated shifts of the E_m in mV, relative to wild-type RCs. Each ΔE_m^{expt} is an average of 3−5 measurements and has a standard error of the mean (SEM) of approximately ±5 mV. Each ΔE_m^{calc} is an average of the results for 5 structures relaxed with P in the reduced state and 5 relaxed in the oxidized state. R, K, E, or D at the mutation site is assumed to be charged while all other ionizable groups are neutral. All the models include a membrane with a 25 Å hydrophobic region. [b] The PDLD calculation of ΔV_{sol} for each structure includes an average over 10 randomly chosen origins for the solvent/membrane grid. The total standard error of the mean (SEM) of ΔE_m^{calc} for each mutant was approximately ±8 mV, including the error associated with choosing the grid origin. [c] The DelPhi calculation of ΔV_{sol} is for 0 M ionic strength, $\epsilon_{in} = 4$, and $\epsilon_{out} = 80$. The SEM of ΔE_m^{calc} for each mutant was approximately ±10 mV.

Calculations. Consider, first, the expected effects of the R(L135) mutations in the absence of dielectric screening. For the mutations R(L135)L and R(L135)E, the changes in the unscreened electrostatic energy difference between P^+ and P ($\Delta\Delta V_{Q\mu}$) are calculated to be −21.6 and −43.7 kcal/mol, respectively, whereas the observed changes in the E_m correspond to only −0.5 and −1.0 kcal/mol. Although P is buried in the intramembrane region of the protein and Arg (L135) also is largely inaccessible to the solvent, the protein, solvent, and electrolytes effectively screen the charge−charge interactions by an average factor of about 40. To explore possible explanations for this strong screening, we calculated the expected effects of the mutations using computational approaches that emphasize several different effects. Because the RC is an integral membrane protein and is purified with a belt of detergents (*72*), most of the models we considered included a 25 Å region with low polarizability sandwiched between two aqueous regions. Relaxations of the polar hydrogen atoms of the protein and crystallographic waters (and, in the MD treatments, any other atoms within a specified region) were treated in the linear-response approximation by averaging ΔV_{sol} over multiple configurations for each oxidation state of P (eq 3). Within the limits of the models, the resulting values of ΔG_{sol} include the free energy change associated with reorganization of the system when P is oxidized (*49*−*52*). Some of the MD simulations also included counterions for the ionizable groups.

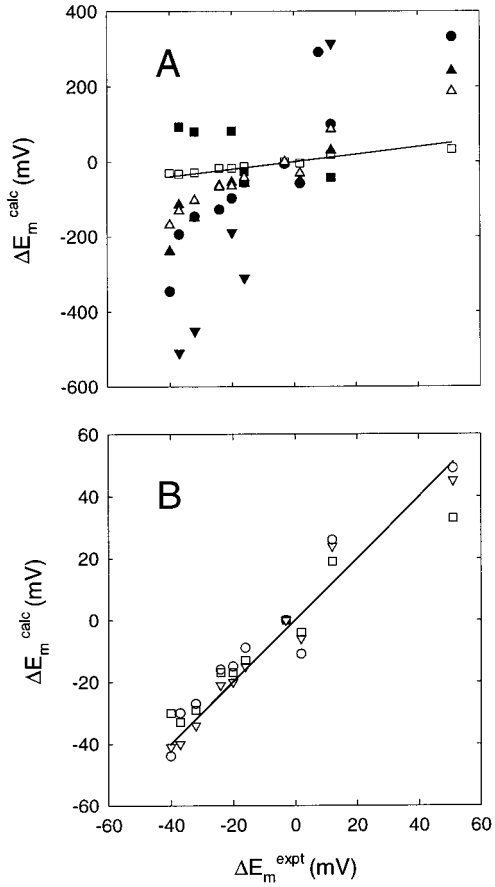

FIGURE 3: Correlation plots of calculated changes of the redox potential (ΔE_m^{calc}) versus the experimental value (ΔE_m^{expt}). For a perfect correlation, the data would fall on the solid line with a slope of 1 and *y*-intercept of 0. (Note that the ordinate and abscissa scales are different.) The ΔE_m^{calc} values are calculated for the charge of P^+ divided equally between P_L and P_M, and are given in mV. (A) The changes in solvation energy were calculated by PDLD (●), DelPhi ($\epsilon_{in} = 4$) (▲), MD without a counterion (▼), MD with a counterion for the mutated residue (■), a linear distance-dependent screening factor ($f_{ij} = r_{ij}$) (△), and an exponential distance-dependent screening factor (eq 8 with $\eta = 0.18$) (□). (B) Expanded view of results for calculations using distance-dependent screening factors given by eq 8 with $\eta = 0.10$ (▽) or 0.18 (□), and by eq 9 (○).

PDLD calculations include an explicit treatment of induced dipoles in the protein and its surroundings. For models with a 25 Å thick membrane, the predicted shifts in the E_m (ΔE_m^{calc}) agree qualitatively with experiment, but overestimate the effects of the mutations by factors of 2−8 (see Table 1 and Figure 3A). Table 2 shows how the calculated ΔE_m for the R(L135)L and R(L135)E mutations depends on the width of the membrane. If the membrane is increased to 40 Å, the protein charges and P^+ are solvated less well, and the predicted shifts of the E_m depart further from the experimental results. A model with no membrane provides the largest screening, as expected, but still overestimates the shift significantly.

PDLD/S treats solvent-induced dipoles explicitly in the same manner as the regular PDLD model, but uses an effective screening factor (ϵ_{in}) for direct charge−charge interactions rather than evaluating induced dipoles in the protein. As mentioned in the introduction, larger values of ϵ_{in} indicate that a greater portion of the overall screening is treated implicitly rather than explicitly. Table 2 includes the calculated values of ΔE_m obtained by PDLD/S calculations for a 25 Å membrane and several values of ϵ_{in}. The best agreement with experiment requires an effective internal dielectric constant of about 20.

Table 2: Shifts in the E_m of P/P^+ in Mutant RCs Calculated by PDLD, PDLD/S, and DelPhi for Various Models of a Membrane and ϵ_{in}[a]

			ΔE_m^{calc}	
model	membrane[b]	ϵ_{in}	R(L135)L	R(L135)E
PDLD	0	−	−73	−134
	25	−	−98	−134
	40	−	−111	−134
PDLD/S	25	2	−106	−212
	25	4	−58	−115
	25	8	−33	−67
	25	20	−19	−38
DelPhi	0	4	−39	−80
	0	20	−20	−40
	25	4	−101	−238
	25	20	−32	−68
	25	40	−20	−40

[a] ΔE_m^{calc} is the calculated change of E_m in mV, relative to wild-type RCs. Each entry is an average of results for 5 structures with P in the reduced state and 5 in the oxidized state. In the PDLD and PDLD/S calculations, 10 randomly chosen origins for the solvent/membrane grid were used for each structure. R or E at the mutation site is assumed to be charged while all other ionizable groups are neutral. The SEM for the PDLD, PDLD/S, and DelPhi calculations are, respectively, ±8, ±8, and ±10 mV. [b] Width of the hydrophobic layer (Å).

The Poisson−Boltzmann (DelPhi) treatment resembles PDLD/S in using a macroscopic ϵ_{in} for charge−charge interactions within the protein. Poisson−Boltzmann calculations with a 25 Å membrane and $\epsilon_{in} = 4$ (a common choice) gave results similar to the PDLD/S treatment with $\epsilon_{in} = 2$, overestimating the effects of the mutations by a factor of 3−6 (Table 2 and Figure 3A). Increasing ϵ_{in} to 40 brought the calculated ΔE_m into reasonable accord with the experimental results (Table 2). A value of 20 for ϵ_{in} is sufficient to reproduce the experimental results in models that do not include a membrane, because P^+ and the ionized residues then are solvated more effectively by the reaction field in the surrounding water.

Table 3 and Figure 3A,B show the shifts in the E_m calculated by using a distance-dependent screening factor for charge−charge interactions. A simple linear function ($f_{ij} = r_{ij}$), which is sometimes used in MD simulations because it avoids the calculation of $\sqrt{r_{ij}}$, greatly underestimates the screening for all the mutations considered here. However, the exponential function with $\eta = 0.10$ or 0.18 (eq 8) and the sigmoidal function (eq 9) both give good agreement with experiment. These simple, empirical expressions predict the experimental results within several millivolts for almost all the mutation sites, including both the surface and buried residues. (As in the PDLD, PDLD/S, and DelPhi calculations, relaxations of polar hydrogen atoms around P and P^+ were treated separately in the linear-response approximation by averaging over 10 structures. However, the ΔE_m values calculated with the exponential or sigmoidal screening function varied little among these structures, giving standard errors of the mean of only ±4 and ±6 mV, respectively.)

Table 3: Shifts in the E_m of P/P$^+$ Calculated with Distance-Dependent Screening Functions and the Linear Response Approximation[a]

		ΔE_m^{calc}			
strain	ΔE_m^{expt}	linear[b]	exponential[c] ($\eta = 0.10$)	exponential[c] ($\eta = 0.18$)	sigmoidal[d]
R(L135)K	−3	0	0	0	0
R(L135)L	−20	−65	−20	−17	−15
R(L135)Q	−24	−68	−21	−17	−16
R(L135)E	−37	−131	−40	−33	−30
D(L155)N	+12	+87	+24	+19	+26
Y(L164)F	+2	−31	−6	−4	−11
R(M164)L	−16	−42	−15	−13	−9
R(M164)E	−32	−103	−34	−29	−27
C(L247)K	+51	+187	+45	+33	+49
C(L247)D	−40	−169	−41	−30	−44
R(L135)E/ C(L247)K	+8	−8	0	0	−10

[a] ΔE_m^{calc} is the calculated change of the E_m in mV, relative to wild-type RCs. Each entry is an average of results for 5 structures with P in the reduced state and 5 in the oxidized state. R, K, E or D at the mutation site is assumed to be charged while all other ionizable groups are neutral. The measured shift for each mutant (ΔE_m^{expt}) is repeated from Table 1 for convenience. [b] $f_{ij} = r_{ij}$. The SEM for each entry is approximately ±15 mV. [c] The exponential screening function given by eq 8. The SEM for each entry is approximately ±4 mV. [d] The sigmoidal screening function given by eq 9. The SEM for each entry is approximately ±6 mV.

Table 4: ΔG_{sol} and λ for P → P$^+$ and the Shift of the E_m of P/P$^+$ Calculated by MD Simulations with and without a Counterion for the Mutated Residue[a]

		without counterion			with counterion[c]		
strain	charge[b]	ΔG_{sol}	λ	ΔE_m^{calc}	ΔG_{sol}	λ	ΔE_m^{calc}
R(L135)R	+1	−24.4	2.4	(0)	−30.6	2.0	(0)
R(L135)L	0	−28.7	1.9	−189	−28.7	1.9	+82
R(L135)E	−1	−36.1	2.0	−510	−28.5	1.6	+93
D(L155)D	−1	−35.2	2.3	(0)	−26.9	2.6	(0)
D(L155)N	0	−27.9	1.7	314	−27.9	1.7	−43
R(M164)R	+1	−24.6	1.7	(0)	−31.2	1.6	(0)
R(M164)L	0	−31.8	1.6	−310	−31.8	1.6	−26
R(M164)E	−1	−35.0	1.2	−451	−29.3	1.6	+80

[a] ΔG_{sol} and λ, the change in solvation free energy and the reorganization energy for the process P → P$^+$, are given in kcal/mol; ΔE_m^{calc} is in mV and is relative to the wild-type model for the residue that was mutated [R(L135)R, D(L155)D, or R(M164)R]. The MD simulations include explicit waters and no membrane. Separate 100 ps trajectories were propagated for P and P$^+$. The root-mean-square fluctuations of ΔV_{sol} in the individual trajectories were approximately 2.8 kcal/mol. [b] Assumed charge of protein without a counterion. Only the residue that was mutated was charged. [c] The MD simulations with a counterion included either a Na^+ or a Cl^- ion in the solvent near the charged residue to make the net charge of the system zero when P was in its reduced state and +1 when P was oxidized.

The results of molecular dynamics (MD) simulations are shown in Figure 3 and are included in Table 4. The calculated shifts of the E_m for models that do not include counterions are similar to those generated by the PDLD calculations. Thus, although they allow the protein and solvent to reorganize more extensively in response to both the mutation and the oxidation of P, the MD simulations without explicit counterions still overestimate the effects of the mutations by a substantial factor.

To examine the effects of counterions, we carried out MD simulations for the wild-type RC and the R(L135), R(M164), and D(L155) mutations with a single Na^+ or Cl^- ion in the water near the mutated or corresponding wild-type residue. Including a counterion brings the predicted shift in the E_m closer to the measured value for all the mutations. In most cases, however, the counterion overcompensates for the change in charge on the protein, so that the sign of the calculated ΔE_m is incorrect (see Table 4). This effect could arise from inappropriate positioning of the counterion closer to P than the ionizable amino acid, possibly because the simulations continued for only 100 ps and included only one ionizable residue in each model. As discussed below, a more accurate treatment probably would have to consider secondary effects involving other ionizable residues and a cloud of electrolytes surrounding the protein. It is interesting nevertheless that the single counterions considered here mainly affected ΔG_{sol} and had relatively little effect on the reorganization energy (λ) associated with the oxidation of P (see Table 4). This indicates that the position of the counterion probably was determined mostly by the ionizable amino acid, and not by the charge on P.

In all the calculations described above, we assumed for simplicity that the positive charge of P$^+$ is distributed equally between P_L and P_M. Measurements of the ENDOR spectrum of P$^+$ have shown that the actual charge in wild-type RCs is greater on P_L than on P_M, and that mutations that alter the number of hydrogen bonds to the two bacteriochlorophylls can change the charge distribution (*44*). ENDOR measurements showed that similar changes of the spin distribution occur in the R(L135)L, R(L135)E, R(M164)L, and R(M164)E mutants described here (E. T. Johnson, W. W. Parson, F. Müh, W. Lubitz, J. C. Williams, J. P. Allen, J. Breton, and E. Nabedryk, unpublished experiments). The estimated ratio of P_L^+ to P_M^+ varied from 1.29 to 3.2 in the order R(M164)E < R(M164)L < wild-type < R(L135)L < R(L135)E. We therefore calculated the expected shifts in the E_m for these mutants using these charge distributions, while retaining the classical picture inherent in eq 2. (As discussed under Materials and Methods, a more refined treatment requires evaluating the electrostatic effects on diabatic $P_L^+P_M$ and $P_LP_M^+$ basis states separately and then rediagonalizing the interaction Hamiltonian. Such an analysis will be presented elsewhere.) As Table 5 shows, calculations using an exponential or sigmoidal distance-dependent screening factor (eqs 8 or 9) still predict the shifts in the E_m well. With these sets of charges, using 0.18 for the exponential factor (η) in eq 8 gives better results than $\eta = 0.10$ for the mutations of R(L135), while the smaller value of η gives somewhat better results for the mutations of R(M164).

DISCUSSION

An underlying assumption in this study is that the ionizable residues at the mutation sites actually are ionized, so that shifts in the E_m of P can be correlated with changes in the charges of the ionized side chains. In agreement with this assumption, the shift of the E_m observed in each of the mutants is qualitatively consistent with the expected effect of changing the charge at that site: the sign of ΔE_m depends on the difference between the signs of the nominal charges of the wild-type and mutant residues, and replacing Arg by a neutral residue (Leu) has approximately half the effect of substituting an oppositely charged amino acid (Glu). The

Table 5: Shifts in the E_m of P/P$^+$ Calculated with Distance-Dependent Screening Functions and Experimentally Measured Charge Distributions[a]

		ΔE_m^{calc}		
strain	ΔE_m^{expt}	exponential[b] ($\eta = 0.10$)	exponential[b] ($\eta = 0.18$)	sigmoidal[c]
R(L135)L	−20	−23	−19	−19
R(L135)E	−37	−48	−39	−40
R(M164)L	−16	−13	−12	−8
R(M164)E	−32	−26	−24	−14

[a] ΔE_m^{calc} is the calculated change of the E_m, in mV, relative to wild-type RCs. The calculations were the same as in Table 3 except for the distribution of charge between P_L and P_M. These calculations were done only for the subset of the mutations for which ENDOR data are available. The ENDOR experiments measure the hyperfine coupling constants of the unpaired electron to nuclear spins on P_L and P_M, which can be related to spin densities and therefore to charge densities on the two bacteriochlorophylls. The wild-type spin density ratio of P_L:P_M is 2.1, and the spin density ratios for the mutations R(L135)E, R(L135)L, R(M164)L, and R(M164)E are, respectively, 3.2, 2.9, 1.6, and 1.3 (E. T. Johnson, W. W. Parson, F. Müh, W. Lubitz, J. C. Williams, J. P. Allen, J. Breton, and E. Nabedryk, unpublished experiments). The measured shifts (ΔE_m^{expt}) are repeated from Table 1 for comparison. [b] The exponential screening function given by eq 8 with $\eta = 0.10$ or 0.18. The SEM for each entry is approximately ±4 mV. [c] The sigmoidal screening function given by eq 9. The SEM for each entry is approximately ±4 mV.

effect of the R(L135)E/C(L247)K double mutation is close to the sum of the effects of the R(L135)E and C(L247)K mutations. The finding that mutations of ionizable groups at several different sites have consistent effects argues that the shifts in the E_m reflect electrostatic interactions rather than structural rearrangements of the protein. The conservative mutations R(L135)K and Y(L164)F, which in principle also could cause structural rearrangements, have no significant effect on the E_m. Additionally, mutations of R(L135) cause slightly larger effects than corresponding mutations of R(M164), in agreement with the small difference between the distances from P on the two sides of the RC and with previous evidence that the charge distribution in P is somewhat asymmetrical.

It is surprising that the charges of buried residues can be reversed without severely destabilizing the RC. The finding that RCs containing an Asp or Lys residue at L247 fold properly is particularly striking, because ionized groups buried in nonpolar surroundings are expected to destabilize proteins. Arginine residues have been shown to stabilize the native conformations of some proteins, and even replacing Arg by Lys can have a destabilizing effect (*73*). Although the mutations described here could have similar destabilizing effects, this might be relatively unimportant if the RC is intrinsically a highly stable protein. The mutant proteins could, however, be stabilized by water molecules that accompany the ionized groups into the nonpolar environment (*15*). The polar hydrogens of Thr (L160) and (L253), Tyr (L164), and several crystalographic waters could reorient to stabilize a negative charge charge at the (L135) site, and similar reorientations of Thr (M289), His (M193), and Glu (M173) could occur around (M164). Charged groups at (L247) could be stabilized by asparagine (M170) and the peptide backbone. As mentioned above, Williams et al. (*16*) recently showed that RCs remain photochemically active when Asn (M199) or (L170) is replaced by an ionized Asp residue. Kirmaier et al. (*74*, *75*) also have introduced Asp and Lys residues close to P without gross disruption of the protein.

We assume also that the average charge of the ionized residue does not change significantly when P is oxidized. In fact, the E_m of P in wild-type *Rb. sphaeroides* RCs decreases slightly with increasing pH between pH 5 and 10, indicating that oxidation of P is coupled to the release of approximately 0.2 proton (*76*, *77*). The residues that account for this proton release have not been identified. Assuming that the protons come exclusively from arginines (L135) and (M164), the change in the average charge at either site would be on the order of −0.1, which would decrease the expected electrostatic effect of a mutation at one of these sites by about 10%. The error would be smaller if the protons come partly from other residues.

The effects of all the mutations on the E_m of P are much smaller than one might have expected, considering the hydrophobic surroundings of P and the fact that most of the residues we mutated have little direct exposure to the solvent. Despite these factors, electrostatic interactions of P with the ionizable residues are screened by an average factor of approximately 40. Depending on the model for the membrane in the PDLD/S and the DelPhi models, this screening corresponds to a macroscopic ϵ_{in} of about 20 for the protein, with the remainder coming from induced dipoles in the surrounding medium. Models that include a membrane region require a larger value for ϵ_{in} to obtain the same amount of screening. As noted in the introduction, electrostatic interactions can be screened by reorientations of O−H, C═O, and N−H dipoles. However, all the electrostatics calculations described in the present work considered ensembles of rotamers of polar hydrogen atoms for each mutant and for each oxidation state of P, and the MD simulations allowed even more extensive rearrangements. The finding that these treatments underestimate the screening badly if counterions are not included in the model argues that movements of protein dipoles are not the dominant source of screening in the present case. It is possible, however, that the MD trajectories were not long enough for complete dipolar reorientation. In particular, they might not reflect the slow reorganization associated with movements of water into or out of the protein. Such movements might occur in response to the mutation, the oxidation of P, or both.

What other processes could account for the strong screening? Perhaps the simplest explanation is that the ionized side chains are accompanied by counterions, which keep the net charge of the system zero. In accord with this view, MD simulations that included explicit counterions predicted smaller shifts of the E_m than simulations that omitted counterions (Table 4). The association of a counterion with the charged residue effectively reduces the charge−charge interactions with P$^+$ to dipolar interactions, which fall off more rapidly with distance. Several previous investigators have found that including counterions increases the stability of MD simulations of proteins (*78*−*80*), although Walser et al. (*81*) recently found no such effect. The divergence of opinion on this point could reflect the difficulty of treating long-range electrostatic interactions. Neutralizing the model probably is the easiest way to obtain a convergent treatment, whether or not counterions are present in the actual system.

A second possibility is that removing or changing the charge of one residue alters the pK_a of one or more other ionizable residues, which then release or bind protons so that the total charge of the protein remains essentially constant. In this case, however, we would expect the effect of a mutation to depend on the constellation of other ionizable residues near the mutation site. Such a dependence might be difficult to detect in water-soluble proteins that have many ionizable residues, but should be more apparent in the RC, where ionizable groups are relatively sparse. Although the effective screening clearly depends on the distance between P and the mutation site, it has no obvious dependence on the proximity of the mutation to other ionizable groups. The guanidino group of Arg (M164), for example, is only 4 Å from the carboxyl group of Glu (M173), whereas the guanidino group of Arg (L135) has no other ionizable groups within 13.5 Å. The distances from Cys (L247) and Asp (L155) to the nearest ionizable group [Arg(L135) in both cases] are 9.3 and 16.0 Å, respectively.

Although microscopic treatments that omit counterions fail to reproduce the effects of the mutations, the effects can be modeled well by using a distance-dependent screening factor that increases from 1 at short interatomic distances to 40 or more at 10 Å. A linear dependence ($f_{ij} = r_{ij}$) proved inadequate in this regard, but the exponential expression used by Warshel et al. (*64*) worked well with either $\eta = 0.1$ or $\eta = 0.18$, as did the sigmoidal function suggested by Hingerty et al. (*65*). The exponential function with $\eta = 0.18$ predicted the effects of mutating the surface residue Asp (L155) more closely than the other functions, although it underestimated the effects of mutating the buried Cys (L247) (see Table 3). Additionally, the exponential function with $\eta = 0.18$ gave somewhat better overall results than the same function with $\eta = 0.10$ in calculations that considered the asymmetrical distribution of charge between the two bacteriochlorophylls of P (Table 5); the difference, however, was marginal. The sigmoidal function overestimated the screening for the Arg (M164) mutants in these last calculations, but worked well for Arg (L135). In part, the similarity of the results obtained with the three functions reflects the spreading of the charge on P^+ across the π-systems of the two bacteriochlorophylls, which leads to a distribution of interatomic distances to the charged atoms of the ionized residues. The major interactions range from about 5 to 15 Å for Cys (L247), 8 to 20 Å for Arg (L135), 12 to 17 Å for Asp (L155), and 12 to 25 Å for Arg (M164). The exponential and sigmoidal functions give similar screening for distances in the region of 10 Å. A critical comparison and parametrization of these functions would require data for both shorter and longer distances, and might be better achieved in systems with more localized charges.

It is remarkable that these empirical functions proved so successful at describing interactions between buried charges in the RC. Distance-dependent screening factors were developed originally from theoretical analyses of saturation effects in ionic solutions (*82*), and were used in proteins to model electrostatic effects on surface residues that were in contact with water and electrolytes (*64*, *65*, *83*). Although Warshel and co-workers have argued that a similar screening occurs in the interior of water-soluble proteins (*64*), one would not necessarily expect the same functions to work well for buried groups in an integral membrane protein. Perhaps the fact that these functions do work well is an indication that protein interiors can accommodate water (*15*) and, in some cases at least, also ions.

Muegge et al. (*22*) have used a discretized-continuum (DelPhi) treatment with $\epsilon_{in} = 1$ to calculate shifts in the E_m of P caused by mutations that add or remove a hydrogen bond with one of the bacteriochlorophylls. Although their results suggest a much weaker screening of electrostatic interactions, they are not necessarily in conflict with ours. As the distance-dependent screening functions (eqs 8 and 9) illustrate, the effective screening factor is expected to be smaller at the short interatomic distances necessary for hydrogen bonding. It is pertinent also that, in the context of classical electrostatics, formation or removal of a hydrogen bond to P^+ amounts to a change in dipole−charge interactions rather than charge−charge interactions, and does not require a counterion to maintain neutrality.

There are, in addition, several differences between the implementation of the discretized-continuum model here and in the work of Muegge et al. (*22*). In the present study, we used the linear-response approximation (eq 3) to incorporate the energy of reorganization of polar hydrogen atoms around P and P^+. Muegge et al. (*22*) minimized the energies of the system separately in the two oxidation states and calculated ΔG_{sol} as

$$\Delta G_{sol} = \langle V_{sol}^{P^+} \rangle_{P^+} - \langle V_{sol}^{P} \rangle_{P} \qquad (11)$$

Here ΔG_{sol}, $\langle V_{sol}^{P^+} \rangle_{P^+}$, and $\langle V_{sol}^{P} \rangle_{P}$ in our notation correspond, respectively, to $-\Delta G$, $G(+)$, and $G(0)$ of Muegge et al. Equation 11 omits the free energy change (λ) associated with rearranging the protein and solvent between their most probable configurations when P is oxidized to P^+. The error probably is small, however, since λ is relatively small and does not change greatly in the mutations considered here (see Table 4).

Whatever the mechanism of the screening, the results presented here support the view that ionized side chains make only small contributions to the electrostatic energies of ion-pair states such as $P^+B_L^-$ and $P^+H_L^-$ in the RC, and thus do not play major roles in establishing the specificity or speed of light-induced charge separation (*35*, *84*). In calculations of such energies, it clearly would be much more accurate to consider all the ionizable residues to be uncharged, rather than to use their nominal charges with a small ϵ_{in}.

ACKNOWLEDGMENT

We thank Drs. JoAnn Williams and Jim Allen for providing the pRKSCH plasmids and *Rb. sphaeroides* ΔLM1.1, and for their help and hospitality during the construction of our first site-directed mutants. Without their guidance, there would not have been nearly so many mutations. We also thank Dr. Steven Boxer for the gift of the pRKSCH/pHis vector and Drs. Arieh Warshel and V. Nagarajan for helpful discussion.

REFERENCES

1. Gilson, M., and Honig, B. (1986) *Biopolymers 25*, 2097−2119.
2. Rees, D. C. (1980) *J. Mol. Biol. 141*, 323−326.
3. Zhou, Z., and Swenson, R. P. (1995) *Biochemistry 34*, 3183−3192.
4. Lockhart, D. J., and Kim, P. S. (1993) *Science 260*, 198−202.

5. Forsyth, W. R., and Robertson, A. D. (2000) *Biochemistry 39*, 8067−8072.
6. Forsyth, W. R., Gilson, M. K., Antosiewicz, J., Jaren, O. R., and Robertson, A. D. (1998) *Biochemistry 37*, 8643−8652.
7. Quiocho, F. A., Sack, J. S., and Vyas, N. K. (1987) *Nature 329*, 561−564.
8. Warshel, A. (1981) *Biochemistry 20*, 3167−3177.
9. Dobson, C. M., Refield, C., and Bartik, K. (1994) *Biophys. J. 66*, 1180−1184.
10. Demchuk, E., Genick, U. K., Woo, T. T., Getzoff, E. D., and Bashford, D. (2000) *Biochemistry 39*, 1100−1113.
11. Åqvist, J., Luecke, H., Quiocho, F. A., and Warshel, A. (1991) *Proc. Natl. Acad. Sci. U.S.A. 88*, 2026−2030.
12. Varadarajan, R., Lambright, D. G., and Boxer, S. G. (1989) *Biochemistry 28*, 3771−3781.
13. Varadarajan, R., Zewert, T. E., Gray, H. B., and Boxer, S. G. (1989) *Science 243*, 69−72.
14. Garcia-Moreno, B., Dwyer, J. J., Gittis, A. G., Lattman, E. E., Spencer, D. S., and Stites, W. E. (1997) *Biophys. Chem. 64*, 211−224.
15. Dwyer, J. J., Gittis, A. G., Karp, D. A., Lattman, E. E., Spencer, D. S., Stites, W. E., and Garcia-Moreno, E. B. (2000) *Biophys. J. 79*, 1610−1620.
16. Williams, J. C., Haffa, A. L., McCulley, J. L., Woodbury, N. W., and Allen, J. P. (2001) *Biochemistry 40*, 15403−15407.
17. Sham, Y. Y., Muegge, I., and Warshel, A. (1998) *Biophys. J. 74*, 1744−1753.
18. Warshel, A., Papazyan, A., and Muegge, I. (1997) *J. Biol. Inorg. Chem. 2*, 143−152.
19. Schutz, C. N., and Warshel, A. (2001) *Proteins: Struct., Funct., Genet. 44*, 400−417.
20. Alexov, E., and Gunner, M. R. (1997) *Biophys. J. 72*, 2075−2093.
21. Sham, Y. Y., Chu, Z. T., and Warshel, A. (1997) *J. Phys. Chem. B 101*, 4458−4472.
22. Muegge, I., Apostolakis, J., Ermler, U., Fritzsch, G., Lubitz, W., and Knapp, E. W. (1996) *Biochemistry 35*, 8359−8370.
23. Langen, R., Brayer, G. D., Berghuis, A. M., McLendon, G., Sherman, F., and Warshel, A. (1992) *J. Mol. Biol. 224*, 589−600.
24. Alexov, E., Miksovska, J., Baciou, L., Schiffer, M., Hanson, D. K., Sebban, P., and Gunner, M. R. (2000) *Biochemistry 39*, 5940−5952.
25. Gunner, M. R., and Alexov, E. (2000) *Biochim. Biophys. Acta 1458*, 63−87.
26. Cutler, R. L., Davies, A. M., Creighton, S., Warshel, A., Moore, G. R., Smith, M., and Mauk, A. G. (1989) *Biochemistry 28*, 3188−3197.
27. Russell, A. J., Thomas, P. G., and Fersht, A. R. (1987) *J. Mol. Biol. 193*, 803−813.
28. Sternberg, M. J., Hayes, F. R., Russell, A. J., Thomas, P. G., and Fersht, A. R. (1987) *Nature 330*, 86−88.
29. Loewenthal, R., Sancho, J., Reinikainen, T., and Fersht, A. R. (1993) *J. Mol. Biol. 232*, 574−583.
30. Antosiewicz, J., McCammon, J. A., and Gilson, M. K. (1994) *J. Mol. Biol. 238*, 415−436.
31. Alexov, E. G., and Gunner, M. R. (1999) *Biochemistry 38*, 8253−8270.
32. Nielsen, J. E., Andersen, K. V., Honig, B., Hooft, R. W., Klebe, G., Vriend, G., and Wade, R. C. (1999) *Protein Eng. 12*, 657−662.
33. Hoff, A. J., and Deisenhofer, J. (1997) *Phys. Rep. 287*, 1−247.
34. Gunner, M., Nichols, A., and Honig, B. (1996) *J. Phys. Chem. 100*, 4277−4291.
35. Alden, R. G., Parson, W. W., Chu, Z. T., and Warshel, A. (1995) *J. Am. Chem. Soc. 117*, 12284−12298.
36. Williams, J. C., Alden, R. G., Murchison, H. A., Peloquin, J. M., Woodbury, N. W., and Allen, J. P. (1992) *Biochemistry 31*, 11029−11037.
37. Lin, X., Murchison, H. A., Nagarajan, V., Parson, W. W., Allen, J. P., and Williams, J. C. (1994) *Proc. Natl. Acad. Sci. U.S.A. 91*, 10265−10270.
38. Allen, J. P., Artz, K., Lin, X., Williams, J. C., Ivancich, A., Albouy, D., Mattioli, T. A., Fetsch, A., Kuhn, M., and Lubitz, W. (1996) *Biochemistry 35*, 6612−6619.
39. Artz, K., Williams, J. C., Allen, J. P., Lendzian, F., Rautter, J., and Lubitz, W. (1997) *Proc. Natl. Acad. Sci. U.S.A. 94*, 13582−13587.
40. Paddock, M. L., Rongey, S. H., Feher, G., and Okamura, M. Y. (1989) *Proc. Natl. Acad. Sci. U.S.A. 86*, 6602−6606.
41. Lin, X., Williams, J. C., Allen, J. P., and Mathis, P. (1994) *Biochemistry 33*, 13517−13523.
42. Goldsmith, J. O., and Boxer, S. G. (1996) *Biochim. Biophys. Acta 1276*, 171−175.
43. Feher, G., and Okamura, M. Y. (1978) in *The Photosynthetic Bacteria* (Clayton, R. K., and Sistrom, W. R., Eds.) pp 349−386, Plenum Press, New York.
44. Rautter, J., Lendzian, F., Schulz, C., Fetsch, A., Kuhn, M., Lin, X., Williams, J. C., Allen, J. P., and Lubitz, W. (1995) *Biochemistry 34*, 8130−8143.
45. Nagarajan, V., Parson, W. W., Davis, D., and Schenck, C. C. (1993) *Biochemistry 32*, 12324−12336.
46. Ermler, U., Fritzsch, G., Buchanan, S. K., and Michel, H. (1994) *Structure 2*, 925−936.
47. Berman, H. M., Westbrook, J., Feng, Z., Gilliland, G., Bhat, T. N., Weissig, H., Shindyalov, I. N., and Bourne, P. E. (2000) *Nucleic Acids Res. 28*, 235−242.
48. Alden, R. G., Parson, W. W., Chu, Z. T., and Warshel, A. (1996) *J. Phys. Chem. 100*, 16761−16770.
49. Lee, F. S., Chu, Z. T., Bolger, M. B., and Warshel, A. (1992) *Protein Eng. 5*, 215−228.
50. Hummer, G., and Szabo, A. (1996) *J. Chem. Phys. 105*, 2004−2010.
51. Sham, Y. Y., Chu, Z. T., Tao, H., and Warshel, A. (2000) *Proteins: Struct., Funct., Genet. 39*, 393−407.
52. Warshel, A., and Parson, W. W. (2001) *Q. Rev. Biophys. 34*, 563−679.
53. Lee, F. S., Chu, Z. T., and Warshel, A. (1993) *J. Comput. Chem. 14*, 161−185.
54. Warshel, A. (1973) *Isr. J. Chem. 11*, 709.
55. Parson, W. W., Nabedryk, E., and Breton, J. (1992) in *The Photosynthetic Bacterial Reaction Center II Structure Spectroscopy, and Dynamics* (Breton, J., and Vermeglio, A., Eds.) pp 79−88, Plenum Press, New York.
56. Parson, W. W., Nagarajan, V., Gaul, D., Schenck, C. C., Chu, Z. T., and Warshel, A. (1990) in *Reaction Centers of Photosynthetic Bacteria* (Michel-Beyerle, M.-E., Ed.) pp 239−249, Springer-Verlag, Berlin.
57. Reimers, J. R., Hughes, J. M., and Hush, N. S. (2000) *Biochemistry 39*, 16185−16189.
58. Gasyna, Z., and Schatz, P. N. (1996) *J. Phys. Chem. 100*, 1445−1448.
59. Warshel, A., and Russell, S. T. (1984) *Q. Rev. Biophys. 17*, 284−290.
60. Klapper, I., Hagstrom, R., Fine, R., Sharp, K., and Honig, B. (1986) *Proteins: Struct., Funct., Genet. 1*, 47−59.
61. Gilson, M., Sharp, K. A., and Honig, B. (1987) *J. Comput. Chem. 9*, 327−335.
62. Nicholls, A., and Honig, B. (1991) *J. Comput. Chem. 12*, 435−445.
63. Sitkoff, D., Sharp, K. A., and Honig, B. (1994) *J. Phys. Chem. 98*, 1978−1988.
64. Warshel, A., Russell, S. T., and Churg, A. K. (1984) *Proc. Natl. Acad. Sci. U.S.A. 81*, 4785−4789.
65. Hingerty, B. E., Ritchie, R. H., Ferrell, T. L., and Turner, J. E. (1985) *Biopolymers 24*, 427−439.
66. Guenot, J., and Kollman, P. A. (1992) *Protein Sci. 1*, 1185−1205.
67. Mehler, E. L., and Guarnieri, F. (1999) *Biophys. J. 77*, 3−22.
68. Parson, W. W., Chu, Z. T., and Warshel, A. (1998) *Biophys. J. 74*, 182−191.
69. Luzhkov, V., and Warshel, A. (1992) *J. Comput. Chem. 13*, 199−213.
70. Lee, F. S., and Warshel, A. (1992) *J. Chem. Phys. 97*, 3100−3107.

71. Lee, B., and Richards, F. M. (1971) *J. Mol. Biol. 55*, 379−400.
72. Roth, M., Arnoux, B., Ducruix, A., and Reiss-Husson, F. (1991) *Biochemistry 30*, 9403−9413.
73. Mrabet, N. T., Van den Broeck, A., Van den brande, I., Stanssens, P., Laroche, Y., Lambeir, A. M., Matthijssens, G., Jenkins, J., Chiadmi, M., van Tilbeurgh, H., Rey, F., Janin, I., Quax, W. J., Lasters, I., Demaeyer, M., and Wodak, S. J. (1992) *Biochemistry 31*, 2239−2253.
74. Heller, B. A., Holten, D., and Kirmaier, C. (1996) *Biochemistry 35*, 15418−15427.
75. Kirmaier, C., Weems, D., and Holten, D. (1999) *Biochemistry 38*, 11516−11530.
76. Maroti, P., and Wraight, C. A. (1988) *Biochim. Biophys. Acta 934*, 314−328.
77. Ivancich, A., Mattioli, T. A., Artz, K., Wang, S., Allen, J. P., and Williams, J. C. (1997) *Biochemistry 36*, 3027−3036.
78. York, D. M., Darden, T. A., Pedersen, L. G., and Anderson, M. W. (1993) *Biochemistry 32*, 1443−1453.
79. Yelle, R. B., Park, N. S., and Ichiye, T. (1995) *Proteins: Struct., Funct., Genet. 22*, 154−167.
80. Ibragimova, G. T., and Wade, R. C. (1998) *Biophys. J. 74*, 2906−2911.
81. Walser, R., Hunenberger, P. H., and van Gunsteren, W. F. (2001) *Proteins: Struct., Funct., Genet. 43*, 509−519.
82. Debye, P. (1929) *Polar Molecules*, Dover, New York.
83. Mehler, E. L., and Eichele, G. (1984) *Biochemistry 23*, 3887−3891.
84. Parson, W. W., Chu, Z. T., and Warshel, A. (1990) *Biochim. Biophys. Acta 1017*, 251−272.
85. Kraulis, P. J. (1991) *J. Appl. Crystallog. 24*, 946−950.
86. Merritt, E. A., and Bacon, D. J. (1997) *Methods Enzymol. 277*, 505−524.

BI012131Y